THE JOURNAL OF PHYSICAL CHEMISTRY C
A JOURNAL OF THE AMERICAN CHEMICAL SOCIETY

pubs.acs.org/JPCC

Article

Positive and Negative Photoconductivity in Monolayer MoS_2 as a Function of Physisorbed Oxygen

Jon K. Gustafson,* Daniel Wines, Ellen Gulian, Can Ataca,* and L. Michael Hayden*

Cite This: *J. Phys. Chem. C* 2021, 125, 8712–8718

Read Online

ACCESS | Metrics & More | Article Recommendations | Supporting Information

ABSTRACT: We investigate the effect of molecular oxygen on the photoconductivity of monolayer MoS_2 via broad-band time-resolved terahertz spectroscopy. We observe that the photoconductivity of monolayer MoS_2 transitions from negative to positive when the environment of MoS_2 changes from vacuum to atmospheric pressure. We argue that this transition from negative to positive photoconductivity results from physically adsorbed oxygen depleting excess electrons from the n-type MoS_2. We attribute the negative photoconductivity to negative trion formation, in which photoinduced excitons capture excess electrons from MoS_2. We attribute the positive photoconductivity to negative trion formation as well; however, in this case, photoinduced excitons capture photoinduced defect electrons rather than excess electrons, which have been immobilized by physisorbed oxygen. These results should prove useful to those who look to make sensors and other types of devices out of monolayer MoS_2 as physisorbed gases, particularly oxygen, can dramatically affect the conductivity of the monolayer.

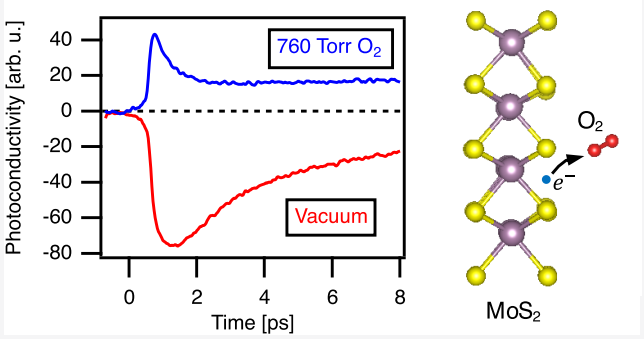

INTRODUCTION

Monolayer transition metal dichalcogenides (TMDs) are two-dimensional (2D) materials of the form MX_2, where M is a transition metal and X is a chalcogen atom. These materials have attracted much interest over the past several years because their unique electronic and optical properties make them suitable for a wide range of device applications.[1,2] Electrically, monolayer TMDs are direct-gap semiconductors with band gaps in the visible range.[3] They are therefore highly attractive for next-generation field-effect transistors (FETs).[4] Optically, monolayer TMDs are dominated by exciton and charged exciton (trion) complexes.[5] Due to spin-valley locking, these excitons and trions are valley dependent, thus making monolayer TMDs promising materials for quantum computing applications, particularly in the field of valleytronics.[6−8]

As researchers continue to look to make devices out of TMDs, it is clear that a complete understanding of how these materials behave is necessary, especially under real-world conditions where the TMDs will interact with external environments. Previous studies have shown that monolayer TMDs are extremely sensitive to molecular gases. Park et al.[9] and Qiu et al.[10] for example report that adsorbed O_2 substantially reduces the current in MoS_2 FETs. Tongay et al.[11,12] and Nan et al.[13] demonstrate that adsorbed gases, such as O_2 and N_2, significantly enhance the photoluminescence of monolayer TMDs. Furthermore, Gogoi et al.[14] report that adsorbed O_2 modulates the dielectric function of monolayer MoS_2. None of these studies however directly measured the effect of O_2 on the photoconductivity of these 2D materials, which may be important for device realization.

We are primarily interested in understanding how O_2 affects the photoconductivity of TMDs. To do so, we utilize time-resolved terahertz spectroscopy (TRTS). TRTS is an experimental technique that allows one to directly probe the photoconductivity of a material. TRTS provides access to the frequency-dependent complex photoconductivity of a material, as well as insight into the dynamics of the photoconductivity with sub-picosecond resolution. A few groups have previously utilized TRTS to study the photoconductivity dynamics of TMDs;[15−21] however, in their work, they have not addressed how O_2 modulates the photoconductivity response of TMDs.

In this paper, we study the effect of O_2 on the THz photoconductivity of chemical vapor deposition (CVD) grown monolayer MoS_2 via broad-band TRTS. We observe that the THz photoconductivity of monolayer MoS_2 changes from negative to positive as the environment of MoS_2 changes from vacuum to 760 Torr of O_2. We attribute this behavior to physically adsorbed O_2 depleting excess electrons from the n-

Received: February 19, 2021
Revised: April 5, 2021
Published: April 16, 2021

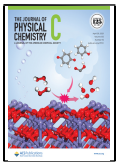

https://doi.org/10.1021/acs.jpcc.1c01550
J. Phys. Chem. C 2021, 125, 8712–8718

type MoS_2. When the monolayer is exposed to vacuum, we observe negative photoconductivity, which we assign to negative trion formation, in which photogenerated excitons combine with excess electrons in the MoS_2. These trions have reduced conductivity due to their increased effective mass. When the monolayer is exposed to oxygen, O_2 physically adsorbs onto the surface of the MoS_2 and excess electrons transfer from the monolayer to O_2, which reduces the base conductivity of the MoS_2 significantly, to a nearly undoped state. With no base conductivity, the conductivity then increases upon photoexcitation. We assign this positive photoconductivity to defect-mediated negative trion formation, in which photoinduced excitons capture photoinduced defect electrons.

EXPERIMENTAL SECTION

Sample Preparation. Our monolayer MoS_2 sample was acquired commercially from 2D Semiconductors.[22] The sample was grown on a sapphire substrate via chemical vapor deposition and then later transferred to a TOPAS (cyclic olefin copolymer) substrate. The sample was slightly n-type.

Time-Resolved Terahertz Spectroscopy. We utilized an optical-pump terahertz probe spectrometer to measure the photoconductivity of monolayer MoS_2. Our TRTS setup is driven by a regeneratively amplified Ti:sapphire laser (Coherent Legend Elite Duo), which generates 30 fs pulses at a 1 kHz repetition rate with a central wavelength of 800 nm. The output of the laser system is split into two beams using a 50/50 beam splitter. One beam is used to pump an optical parametric amplifier (Coherent OperA Solo), which allows for tunable excitation pulses. The excitation beam diameter is roughly 2 mm. The other beam is then split again: one beam for terahertz generation and one for terahertz detection. Broadband terahertz pulses are generated using a two-color, air-plasma technique,[23] where 800 nm light is focused through a BBO crystal and the fundamental and second harmonic are mixed in an air-plasma filament. Terahertz pulses are detected using electro-optic sampling[24] in a 300 μm thick GaP crystal, which provides continuous bandwidth from 0.5 to 8 THz.[25,26] The terahertz beam diameter is roughly 800 μm at the sample. The entire beam path is purged with dry air to avoid water vapor absorption.

RESULTS AND DISCUSSION

In Figure 1, we present the ultraviolet−visible (UV−vis) absorption spectrum of our monolayer MoS_2 film at room temperature. Similar to others,[16,18] we observe three resonances in the absorption spectrum, which correspond to the A, B, and C excitons. The A, B, and C excitons are located at 643 nm (1.93 eV), 600 nm (2.07 eV), and 429 nm (2.89 eV) respectively.

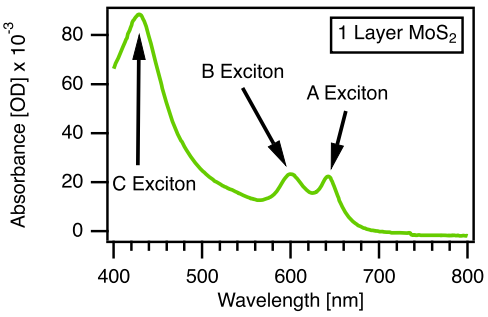

Figure 1. Ultraviolet−visible absorbance spectrum of monolayer MoS_2 on TOPAS (cyclic olefin copolymer) substrate at 300 K. Peaks A, B, and C denote the different exciton resonances.

To probe the effect of O_2 on the photoinduced conductivity dynamics of our monolayer MoS_2 sample, we utilized TRTS. Here, we measured the fractional change in transmission of the peak of the terahertz waveform ($\Delta E/E_0$) as a function of time after pump excitation when the MoS_2 was in vacuum and when MoS_2 was in 760 Torr of O_2. For both experiments, the MoS_2 was pumped on resonance with the A exciton at 300 K (643 nm). In vacuum (Figure 2a), we observed an ultrafast increase

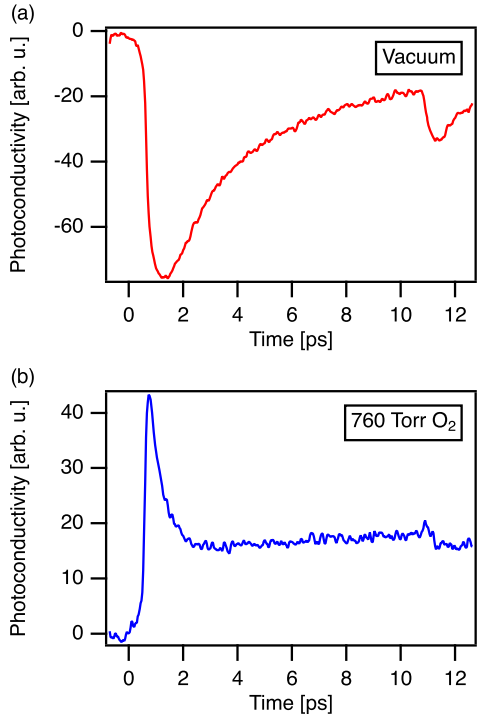

Figure 2. Terahertz photoconductivity $\Delta\sigma \sim -\Delta E/E_0$ of monolayer MoS_2 in (a) vacuum and in (b) 760 Torr of O_2 as a function of time after pump excitation. The sample is photoexcited on resonance with the A exciton at 300 K (643 nm) with an incident fluence of ~4.5 × 10^{14} photons/cm^2.

in $\Delta E/E_0$ upon photoexcitation, indicating a photoinduced decrease in conductivity, since the photoconductivity, $\Delta\sigma \sim -\Delta E/E_0$. Following the decrease, the conductivity then recovered on a timescale on the order of several picoseconds. In the oxygen environment (Figure 2b), we observed an ultrafast decrease in $\Delta E/E_0$ upon photoexcitation, indicating a photoinduced increase in conductivity. Following the increase, the conductivity then decayed rapidly within 1 ps to a nonzero level that persisted for over 200 ps. In both the vacuum and oxygen MoS_2 photoconductivity dynamics, we observed a slight decrease in the photoconductivity of MoS_2 ~10.5 ps after photoexcitation, which we attribute to a pump beam reflection off of the TOPAS substrate re-photoexciting the MoS_2. We also observed that the switch between negative and positive photoconductivity is reversible.

To understand the photoinduced decrease in conductivity described in Figure 2a, we consider the role of doping in monolayer MoS_2. Previous work reports that monolayer MoS_2 grown via chemical vapor deposition is n-type (has excess

https://doi.org/10.1021/acs.jpcc.1c01550
J. Phys. Chem. C 2021, 125, 8712−8718

electrons).[27] Given that mobile electrons absorb THz radiation, we therefore expect our MoS_2 sample to have a base conductivity that is proportional to the excess electron concentration. Upon photoexcitation, we generate excitons in the MoS_2 since we photoexcite the sample with photons of the same energy as the A exciton. Therefore, immediately after photoexcitation, the MoS_2 has an exciton population in addition to the excess electron population. Due to enhanced Columbic interactions, we expect the excess electrons to bind to the photogenerated excitons almost instantaneously[15,28] to form negative trions. Trions, being three-body systems, have a higher effective mass than electrons and thus a lower mobility and conductivity. Since trions, which dominate the conductivity after photoexcitation, have lower conductivity than electrons, which dominate the conductivity before photoexcitation, the measured photoconductivity (the change in conductivity) of MoS_2 is negative. Lui et al. report negative photoconductivity in monolayer MoS_2 due to negative trion formation as well.[15]

To understand the photoinduced increase in conductivity described in Figure 2b, we consider the effect of oxygen on MoS_2. Previous work reports that when O_2 is adsorbed onto the surface of MoS_2, charge transfers from MoS_2 to O_2.[11,12,29−32] We therefore expect the density of excess electrons in our n-type MoS_2 sample to decrease when oxygen is introduced to the environment of the MoS_2. This depletion of excess charge consequently reduces the base conductivity of the MoS_2, nearly to an undoped level, depending on the oxygen coverage and the original doping level. Upon on-resonance photoexcitation, we generate a population of excitons; however, unlike before when the MoS_2 was in vacuum, we do not have a population of excess electrons for the excitons to form negative trions with because of O_2 adsorption. Furthermore, excitons themselves do not contribute strongly to the THz conductivity since they are charge neutral and have binding energies outside of our experimental window. To understand the increase in conductivity, we also consider the role defects play in the system. In CVD-grown monolayer MoS_2, sulfur vacancies, the most prominent type of defect,[33,34] introduce states within the band gap.[35] The energy supplied by the on-resonance pump beam can promote electrons trapped in these defect states to the conduction band. These photoinduced defect electrons can then bind to the photogenerated excitons to form negative trions. Since the base conductivity of the MoS_2 is reduced due to O_2 adsorption, the conductivity after photoexcitation, which is determined by the negative trions, is greater than the conductivity before photoexcitation. The measured photoconductivity (change in conductivity) of MoS_2 is therefore positive.

We attribute the decay of the negative and positive photoconductivity to defects. This is because trions decay predominately through defect-mediated processes.[15,20] In this decay mechanism, trions become trapped in defect states that are located in the band gap and thus no longer contribute to the conductivity. The picosecond timescale decay we observe in the negative photoconductivity and the sub-picosecond timescale decay we observe in the positive photoconductivity support this defect-mediated decay mechanism. When the photoconductivity is positive, trion formation is defect-mediated. Electrons are promoted from defect states to the conduction band so that they can then bind to photogenerated excitons to form trions. Defect states are now unoccupied and can thus trap trions. When the photoconductivity is negative, trions form when excess electrons in the conduction band bind to photogenerated excitons. This process is not defect-mediated; however, defects still play a role in the photoconductivity in the sense that the excitation pulse promotes electrons in defect states to the conduction band, which leaves defect states unoccupied to trap trions. Since the conduction band is initially occupied though with excess electrons, fewer defect electrons can be photoexcited than when the photoconductivity is positive, in which the conduction band is unoccupied. Since there are fewer states available to trap trions, the negative photoconductivity should decay slower than the positive photoconductivity, which is what we observe.

We attribute the long-lived photoconductivity observed when monolayer MoS_2 is in oxygen to photoinduced oxygen desorption. From kinetic theory, it is known that as temperature increases, the rate of O_2 desorption increases. In our TRTS experiments, the excitation pulse increases the temperature of the MoS_2 (see the Supporting Information for a discussion on the laser heating effect). Therefore, upon photoexcitation, we expect some O_2 to get desorbed from the surface of the MoS_2. As these O_2 molecules are desorbed, depleted electrons transfer back to the MoS_2 and therefore increase the MoS_2 conductivity. Since there are no holes for these electrons to relax to (because these electrons were not photoexcited from the valence band), the photoconductivity persists. From 2 to 10 ps after photoexcitation, the photoconductivity actually rises slightly instead of decaying because oxygen is still desorbing from the surface. The decrease in the photoconductivity we observe at around 10.5 ps after photoexcitation supports this idea that electrons dominate the long-lived photoconductivity, through the following argument. As mentioned earlier, the decrease in the photoconductivity at around 10.5 ps after photoexcitation occurs because a pump beam reflection off of the TOPAS substrate re-photoexcites the MoS_2. We know from the previous discussion that MoS_2 exhibits a photoinduced decrease in conductivity when MoS_2 is n-type. Since the pump reflection causes a photoinduced decrease in the conductivity, the MoS_2 at the time of the reflection must then be n-type, which suggests that electrons determine the long-lived photoconductivity.

We also looked at the effect of temperature on the long-lived photoconductivity of monolayer MoS_2 in oxygen. In Figure 3, we present the photoconductivity dynamics of monolayer

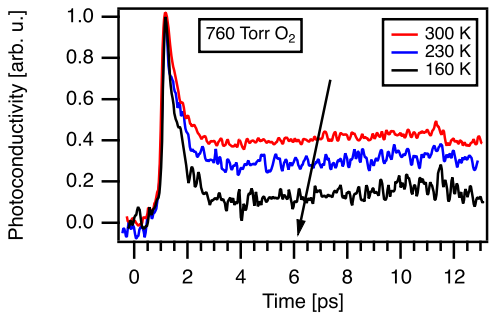

Figure 3. Terahertz photoconductivity of monolayer MoS_2 as a function of time after photoexcitation at 300 K (red trace), 230 K (blue trace), and 160 K (black trace). The sample is pumped on resonance with the A exciton (643 nm at 300 K, 626 nm at 230 K, and 616 nm at 160 K) with an incident fluence of ~4.5 × 10^{14} photons/cm^2.

https://doi.org/10.1021/acs.jpcc.1c01550
J. Phys. Chem. C 2021, 125, 8712−8718

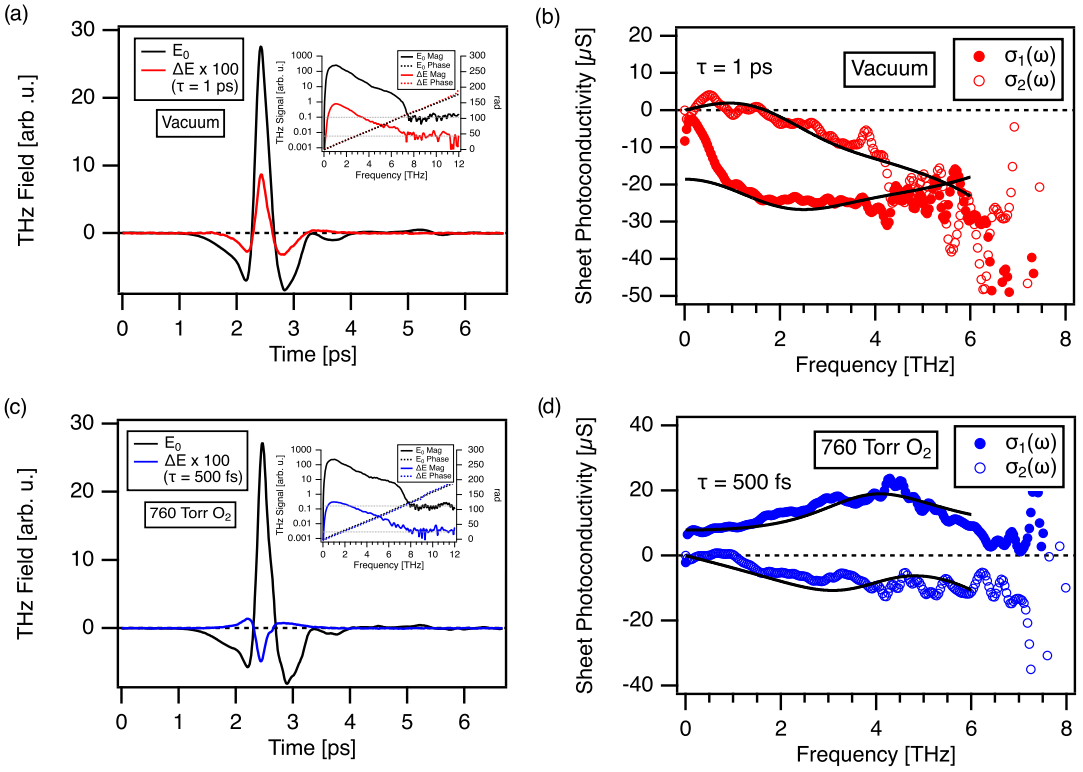

Figure 4. THz waveform $E_0(t)$ (black traces) and the pump-induced modulation of the THz waveform $\Delta E(t)$ of monolayer MoS_2 in (a) vacuum (red trace) and in (c) 760 Torr of O_2 (blue trace). The insets plot the Fourier transforms of $E_0(t)$ and $\Delta E(t)$ (solid (dashed) lines are the magnitudes (phases) of the transforms and dotted gray lines are the noise floors for the respective spectra). The complex frequency-dependent sheet photoconductivity of monolayer MoS_2 in (b) vacuum and in (d) 760 Torr of O_2 at 1 ps and 500 fs after photoexcitation, respectively. The MoS_2 is pumped on resonance with the A exciton at 300 K (643 nm). The absorbed fluence is $\sim 2.4 \times 10^{13}$ photons/cm^2. The solid (open) circles are the real (imaginary) part of the induced photoconductivity. The solid lines over the circles represent fits to the photoconductivity.

MoS_2 in 760 Torr of O_2 at 300, 230, and 160 K normalized to their respective peaks. At all three temperatures, we excited the MoS_2 on resonance with the A exciton (see the Supporting Information for the A exciton's temperature dependence). From these measurements, we find that the long-lived photoconductivity decreases as the temperature decreases. This behavior supports the photoinduced oxygen desorption mechanism described above. As the temperature decreases, fewer oxygen molecules desorb from the surface of the MoS_2 upon photoexcitation and, thus, fewer electrons transfer back to the MoS_2. With fewer electrons in the MoS_2, the long-lived photoconductivity, which is due to these electrons, then decreases.

To further investigate the effect of O_2 on the photoconductivity of monolayer MoS_2, we extracted the complex frequency-dependent sheet photoconductivity by recording the entire fractional pump-induced modulation of the terahertz waveform (Figure 4a,c) using our TRTS spectrometer (see the Supporting Information for details on calculating the complex sheet photoconductivity). In Figure 4b, we present the sheet photoconductivity of monolayer MoS_2 in vacuum at 1 ps after photoexcitation. In Figure 4d, we present the sheet photoconductivity of monolayer MoS_2 in oxygen at 500 fs after photoexcitation. We excited the MoS_2 on resonance with the A exciton at 300 K for both of these sheet photoconductivity measurements. In vacuum, we find that both the real and imaginary parts of the photoconductivity are negative. In the oxygen environment, we find that the real part of the photoconductivity is positive and the imaginary part of the photoconductivity is negative. In an effort to understand these frequency-dependent photoconductivity curves, we employ a multicomponent model (see the Supporting Information).

For MoS_2 in vacuum, we know from the previous discussion that the conductivity after photoexcitation is attributed to negative trions and that the conductivity before photoexcitation is attributed to excess electrons. Therefore, we model the sheet photoconductivity as $\Delta\sigma = \sigma_t - \sigma_e$, where σ_t is the conductivity due to the trions and σ_e is the conductivity due to the excess electrons. Our previous work[20] showed that trions in TMDs contribute to the conductivity in three ways: a Drude response, a broad resonance response due to charge buildup at grain boundaries, and a dissociation response at the trion binding energy. For the trion component σ_t, we model the conductivity with these three responses. For the electron component σ_e, we model the conductivity with only a Drude response and a broad resonance response. In the Supporting Information, we provide more details on this fit function, as well as a table with the resulting fit parameters. In Figure 4b, we plot the fit to the real and imaginary parts of the sheet photoconductivity (black traces). We find that our model agrees very well with the data, thus further confirming that the negative photoconductivity of monolayer MoS_2 in vacuum is due to the negative trion formation mechanism described earlier.

For MoS_2 in oxygen (Figure 4d), we know from the previous discussion that the conductivity after photoexcitation is due to negative trions and that the conductivity before photoexcitation is negligible since oxygen adsorption depletes excess

https://doi.org/10.1021/acs.jpcc.1c01550
J. Phys. Chem. C 2021, 125, 8712−8718

electrons from MoS_2. We therefore model the sheet photoconductivity with just a trion component, $\Delta\sigma = \sigma_t$. Here, σ_t has a Drude response, a broad resonance response, and a dissociation response. In the Supporting Information, we provide the fitting function, as well as a table with the resulting fit parameters. In Figure 4d, we plot the fit to the real and imaginary parts of the sheet photoconductivity (black traces). We again find that the fit models the data very well, which further verifies that the positive photoconductivity of monolayer MoS_2 in oxygen is a consequence of oxygen adsorption depleting excess electrons from the MoS_2. The resulting fit also confirms the defect-mediated nature of trion formation that occurs when MoS_2 is in an oxygen environment. From Table S2, we find that the total trion concentration is roughly half of the absorbed fluence. In the defect-mediated trion formation mechanism discussed earlier, a trion forms when an electron is photoexcited from a defect state located in the band gap to the conduction band and then binds to a photogenerated exciton. Two photons are required to form one trion (one to promote an electron to the conduction band and one to create an exciton). Therefore, the total trion concentration should be one-half of the absorbed fluence.

To better understand the charge transfer process between MoS_2 and adsorbed O_2, we simulated the interaction between monolayer MoS_2 and O_2 using density functional theory (DFT) and ab initio molecular dynamics (MD). From these calculations, we find that up to 0.2 electrons per O_2 molecule can transfer from the MoS_2 to the physically adsorbed oxygen (see the Supporting Information for more details). We then applied a Langmuir adsorption model to estimate the amount of oxygen adsorbed on the surface of the MoS_2. For steady-state physical adsorption, the fraction of adsorption sites occupied by O_2 molecules, θ, is given by

$$\theta = \frac{1}{1 + \frac{\upsilon_{des} N}{F} e^{-(E_{des} - E_a)/kT}} \quad (1)$$

where υ_{des} is the attempt frequency, N is the density of adsorption sites, F is the gas impingement flux, E_{des} is the desorption energy, E_a is the activation energy, k is Boltzmann's constant, and T is the temperature. The attempt frequency is given by $\upsilon_{des} = kT/h$, where h is Planck's constant. The gas impingement flux is represented by $F = P/\sqrt[2]{2\pi mkT}$, where P is the gas pressure and m is the molecular mass. Setting P = 760 Torr, T = 300 K, E_a = 0 meV, E_{des} = 126 meV, $m = 5.31 \times 10^{-26}$ kg, and $N = 7.1 \times 10^{13}$ cm^{-2} (corresponding to one site per 4 × 4 supercell), we calculate that θ = 0.076 and therefore estimate the amount of oxygen adsorbed on our sample, given by $\theta \times N$, to be roughly 5.3×10^{12} cm^{-2}. Given this oxygen coverage of ~5.3×10^{12} cm^{-2} and knowing that 0.2 electrons transfer per O_2 molecule, we then calculate the total charge transfer. By multiplying 5.3×10^{12} cm^{-2} and 0.2 electrons per O_2, we estimate the concentration of electrons that transfer from the MoS_2 to oxygen to be approximately 1.1×10^{12} cm^{-2}. This value of 1.1×10^{12} cm^{-2} is comparable to the estimated doping level of our n-type MoS_2 sample, 3.1×10^{12} cm^{-2}, which indicates that the adsorbed O_2 significantly depletes electrons from our MoS_2 sample. This significant depletion explains why we experimentally observe a dramatic change in the photoconductivity (from negative to positive) upon introducing 760 Torr of O_2 to our sample.

At lower oxygen pressures, we calculate that there is insufficient O_2 coverage to deplete all of the electrons from the MoS_2. To investigate the photoconductivity at this reduced doping state (exhibited at low O_2 pressures), we measured the THz photoconductivity dynamics as we pulled a vacuum on the sample (shown in Figure 5). In Figure 5, we observe that

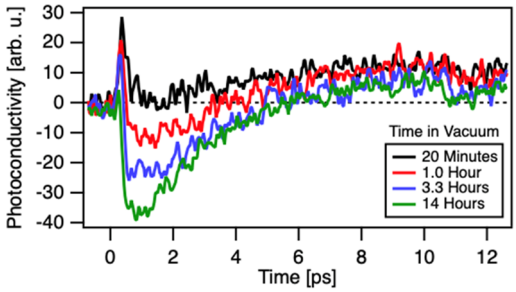

Figure 5. Terahertz photoconductivity dynamics of monolayer MoS_2 after 20 min in vacuum (black trace), 1 h in vacuum (red trace), 3.3 h in vacuum (blue trace), and 14 h in vacuum (green trace). The MoS_2 is pumped on resonance with the A exciton at 300 K (643 nm) with an incident fluence of ~4.5×10^{14} photons/cm^2.

the photoconductivity has both a positive and negative component. Furthermore, we find that as we pull a vacuum (O_2 coverage decreases), the positive photoconductivity decreases while the magnitude of the negative photoconductivity increases. This behavior is a consequence of the competition between defect-mediated trion formation (responsible for the positive photoconductivity) and trion formation due to photogenerated excitons capturing excess charge from the monolayer (responsible for the negative photoconductivity).

CONCLUSIONS

In summary, we have shown using broad-band TRTS that when the environment of monolayer MoS_2 changes from vacuum to 760 Torr of O_2, the photoconductivity changes from negative to positive. We find that this behavior is a consequence of physically adsorbed O_2 depleting excess electrons from the n-type MoS_2. In vacuum, excess electrons bind to photogenerated excitons to form negative trions that have reduced conductivity. In oxygen, photoexcited defect electrons bind to photogenerated excitons to form negative trions that increase the conductivity. Further analysis shows that photoinduced O_2 desorption creates a long-lived conductivity in MoS_2 that is dominated by electrons that transfer back to the MoS_2. This long-lived photoconductivity component does not occur when MoS_2 is in vacuum since no oxygen is present before photoexcitation. These results and analysis provide valuable insight into the effect of O_2 on the photoconductivity of MoS_2 and therefore should be useful to those who look to make devices out of MoS_2 and point to the need to potentially passivate the effects of adsorbed gases on TMD monolayers.

ASSOCIATED CONTENT

Supporting Information

The Supporting Information is available free of charge at https://pubs.acs.org/doi/10.1021/acs.jpcc.1c01550.

Discussion on laser heating, details concerning the measurement of the temperature-dependent absorption spectrum, details on the calculation of the photoconductivity, a discussion on fitting the photoconduc-

https://doi.org/10.1021/acs.jpcc.1c01550
J. Phys. Chem. C 2021, 125, 8712−8718

tivity, details about the computational methods, adsorption and charge transfer calculations, molecular dynamics results, density of states calculations, and charge density difference calculations at different coverages (PDF)

AUTHOR INFORMATION

Corresponding Authors

Jon K. Gustafson − *Department of Physics, UMBC, Baltimore, Maryland 21250, United States;* orcid.org/0000-0003-1745-3121; Email: jgus1@umbc.edu

Can Ataca − *Department of Physics, UMBC, Baltimore, Maryland 21250, United States;* orcid.org/0000-0003-4959-1334; Email: ataca@umbc.edu

L. Michael Hayden − *Department of Physics, UMBC, Baltimore, Maryland 21250, United States;* Email: hayden@umbc.edu

Authors

Daniel Wines − *Department of Physics, UMBC, Baltimore, Maryland 21250, United States;* orcid.org/0000-0003-3855-3754

Ellen Gulian − *Department of Physics, UMBC, Baltimore, Maryland 21250, United States*

Complete contact information is available at: https://pubs.acs.org/10.1021/acs.jpcc.1c01550

Notes

The authors declare no competing financial interest.

ACKNOWLEDGMENTS

J.K.G. and L.M.H. acknowledge support from a UMBC START grant. J.K.G. also acknowledges the support of the Department of Education through a GAANN Fellowship under award number P200A150003-17. E.G. acknowledges support from a UMBC URA Scholarship. D.W. and C.A. acknowledge support by the National Science Foundation through the Division of Materials Research under NSF DMR-1726213 Grant.

REFERENCES

(1) Xia, F. N.; Wang, H.; Xiao, D.; Dubey, M.; Ramasubramaniam, A. Two-Dimensional Material Nanophotonics. *Nat. Photonics* **2014**, *8*, 899−907.

(2) Mak, K. F.; Shan, J. Photonics and Optoelectronics of 2D Semiconductor Transition Metal Dichalcogenides. *Nat. Photonics* **2016**, *10*, 216−226.

(3) Yun, W. S.; Han, S. W.; Hong, S. C.; Kim, I. G.; Lee, J. D. Thickness and Strain Effects on Electronic Structures of Transition Metal Dichalcogenides: 2H-MX_2 Semiconductors (M = Mo, W; X = S, Se, Te). *Phys. Rev. B* **2012**, *85*, No. 033305.

(4) Radisavljevic, B.; Radenovic, A.; Brivio, J.; Giacometti, V.; Kis, A. Single-Layer MoS_2 Transistors. *Nat. Nanotechnol.* **2011**, *6*, 147−150.

(5) Wang, G.; Chernikov, A.; Glazov, M. M.; Heinz, T. F.; Marie, X.; Amand, T.; Urbaszek, B. Colloquium: Excitons in Atomically Thin Transition Metal Dichalcogenides. *Rev. Mod. Phys.* **2018**, *90*, No. 021001.

(6) Liu, Y. P.; Gao, Y. J.; Zhang, S. Y.; He, J.; Yu, J.; Liu, Z. W. Valleytronics in Transition Metal Dichalcogenides Materials. *Nano Res.* **2019**, *12*, 2695−2711.

(7) Xiao, D.; Liu, G. B.; Feng, W. X.; Xu, X. D.; Yao, W. Coupled Spin and Valley Physics in Monolayers of MoS_2 and Other Group-VI Dichalcogenides. *Phys. Rev. Lett.* **2012**, *108*, No. 196802.

(8) Mak, K. F.; He, K. L.; Shan, J.; Heinz, T. F. Control of Valley Polarization in Monolayer MoS_2 by Optical Helicity. *Nat. Nanotechnol.* **2012**, *7*, 494−498.

(9) Park, W.; Park, J.; Jang, J.; Lee, H.; Jeong, H.; Cho, K.; Hong, S.; Lee, T. Oxygen Environmental and Passivation Effects on Molybdenum Disulfide Field Effect Transistors. *Nanotechnology* **2013**, *24*, No. 095202.

(10) Qiu, H.; Pan, L.; Yao, Z.; Li, J.; Shi, Y.; Wang, X. Electrical Characterization of Back-Gated Bi-Layer MoS_2 Field-Effect Transistors and the Effect of Ambient on Their Performances. *Appl. Phys. Lett.* **2012**, *100*, No. 123104.

(11) Tongay, S.; Zhou, J.; Ataca, C.; Liu, J.; Kang, J. S.; Matthews, T. S.; You, L.; Li, J.; Grossman, J. C.; Wu, J. Broad-Range Modulation of Light Emission in Two-Dimensional Semiconductors by Molecular Physisorption Gating. *Nano Lett.* **2013**, *13*, 2831−2836.

(12) Tongay, S.; Suh, J.; Ataca, C.; Fan, W.; Luce, A.; Kang, J. S.; Liu, J.; Ko, C.; Raghunathanan, R.; Zhou, J.; Ogletree, F.; Li, J. B.; Grossman, J. C.; Wu, J. Defects Activated Photoluminescence in Two-Dimensional Semiconductors: Interplay Between Bound, Charged, and Free Excitons. *Sci. Rep.* **2013**, *3*, No. 2657.

(13) Nan, H. Y.; Wang, Z. L.; Wang, W. H.; Liang, Z.; Lu, Y.; Chen, Q.; He, D. W.; Tan, P. H.; Miao, F.; Wang, X. R.; Wang, J. L.; Ni, Z. H. Strong Photoluminescence Enhancement of MoS_2 through Defect Engineering and Oxygen Bonding. *ACS Nano* **2014**, *8*, 5738−5745.

(14) Gogoi, P. K.; Hu, Z. L.; Wang, Q. X.; Carvalho, A.; Schmidt, D.; Yin, X. M.; Chang, Y. H.; Li, L. J.; Sow, C. H.; Neto, A. H. C.; Breese, M. B. H.; Rusydi, A.; Wee, A. T. S. Oxygen Passivation Mediated Tunability of Trion and Excitons in MoS_2. *Phys. Rev. Lett.* **2017**, *119*, No. 077402.

(15) Lui, C. H.; Frenzel, A. J.; Pilon, D. V.; Lee, Y.-H.; Ling, X.; Akselrod, G. M.; Kong, J.; Gedik, N. Trion-Induced Negative Photoconductivity in Monolayer MoS_2. *Phys. Rev. Lett.* **2014**, *113*, No. 166801.

(16) Docherty, C. J.; Parkinson, P.; Joyce, H. J.; Chiu, M.; Chen, C.; Lee, M.; Li, L.; Herz, L. M.; Johnston, M. B. Ultrafast Transient Terahertz Conductivity of Monolayer MoS_2 and WSe_2 Grown by Chemical Vapor Deposition. *ACS Nano* **2014**, *8*, 11147−11153.

(17) Kar, S.; Su, Y.; Nair, R. R.; Sood, A. K. Probing Photoexcited Carriers in a Few-Layer MoS_2 Laminate by Time-Resolved Optical Pump-Terahertz Probe Spectroscopy. *ACS Nano* **2015**, *9*, 12004−12010.

(18) Cunningham, P. D.; McCreary, K. M.; Hanbicki, A. T.; Currie, M.; Jonker, B. T.; Hayden, L. M. Charge Trapping and Exciton Dynamics in Large-Area CVD Grown MoS_2. *J. Phys. Chem. C* **2016**, *120*, 5819−5826.

(19) Xing, X.; Zhao, L. T.; Zhang, Z. Y.; Liu, X. K.; Zhang, K. L.; Yu, Y.; Lin, X.; Chen, H. Y.; Chen, J. Q.; Jin, Z. M.; Xu, J. H.; Ma, G. H. Role of Photoinduced Exciton in the Transient Terahertz Conductivity of Few-Layer WS_2 Laminate. *J. Phys. Chem. C* **2017**, *121*, 20451−20457.

(20) Gustafson, J. K.; Cunningham, P. D.; McCreary, K. M.; Jonker, B. T.; Hayden, L. M. Ultrafast Carrier Dynamics of Monolayer WS_2 via Broad-Band Time-Resolved Terahertz Spectroscopy. *J. Phys. Chem. C* **2019**, *123*, 30676−30683.

(21) Liu, X. F.; Yu, H. Y.; Ji, Q. Q.; Gao, Z. H.; Ge, S. F.; Qiu, J.; Liu, Z. F.; Zhang, Y. F.; Sun, D. An Ultrafast Terahertz Probe of the Transient Evolution of the Charged and Neutral Phase of Photo-Excited Electron-Hole Gas in a Monolayer Semiconductor. *2D Mater.* **2016**, *3*, No. 014001.

(22) 2D Semiconductor CVD MoS_2 Monolayers. https://www.2dsemiconductors.com/full-area-coverage-monolayer-mos2-on-c-cut-sapphire/ (accessed April 1, 2021).

(23) Xie, X.; Dai, J. M.; Zhang, X. C. Coherent Control of THz Wave Generation in Ambient Air. *Phys. Rev. Lett.* **2006**, *96*, No. 075005.

(24) Planken, P. C. M.; Nienhuys, H. K.; Bakker, H. J.; Wenckebach, T. Measurement and Calculation of the Orientation Dependence of Terahertz Pulse Detection in ZnTe. *J. Opt. Soc. Am. B* **2001**, *18*, 313−317.

(25) Wu, Q.; Zhang, X. C. 7 Terahertz Broadband GaP Electro-Optic Sensor. *Appl. Phys. Lett.* **1997**, *70*, 1784−1786.
(26) Chakkittakandy, R.; Corver, J.; Planken, P. C. M. Quasi-Near Field Terahertz Generation and Detection. *Opt. Express* **2008**, *16*, 12794−12805.
(27) Lee, Y. H.; Zhang, X. Q.; Zhang, W. J.; Chang, M. T.; Lin, C. T.; Chang, K. D.; Yu, Y. C.; Wang, J. T. W.; Chang, C. S.; Li, L. J.; Lin, T. W. Synthesis of Large-Area MoS_2 Atomic Layers with Chemical Vapor Deposition. *Adv. Mater.* **2012**, *24*, 2320−2325.
(28) Steinleitner, P.; Merkl, P.; Nagler, P.; Mornhinweg, J.; Schuller, C.; Korn, T.; Chernikov, A.; Huber, R. Direct Observation of Ultrafast Exciton Formation in a Monolayer of WSe_2. *Nano Lett.* **2017**, *17*, 1455−1460.
(29) Liu, H.; Han, N.; Zhao, J. Atomistic Insight into the Oxidation of Monolayer Transition Metal Dichalcogenides: From Structures to Electronic Properties. *RSC Adv.* **2015**, *5*, 17572−17581.
(30) Liu, Y.; Stradins, P.; Wei, S. Air Passivation of Chalcogen Vacancies in Two-Dimensional Semiconductors. *Angew. Chem., Int. Ed.* **2016**, *55*, 965−968.
(31) Yue, Q.; Shao, Z.; Chang, S.; Li, J. Adsorption of Gas Molecules on Monolayer MoS_2 and Effect of Applied Electric Field. *Nanoscale Res. Lett.* **2013**, *8*, No. 425.
(32) Qi, L.; Wang, Y.; Shen, L.; Wu, Y. H. Chemisorption-Induced n-Doping of MoS_2 by Oxygen. *Appl. Phys. Lett.* **2016**, *108*, No. 063103.
(33) Hong, J. H.; Hu, Z. X.; Probert, M.; Li, K.; Lv, D. H.; Yang, X. N.; Gu, L.; Mao, N. N.; Feng, Q. L.; Xie, L. M.; Zhang, J.; Wu, D. Z.; Zhang, Z. Y.; Jin, C. H.; Ji, W.; Zhang, X. X.; Yuan, J.; Zhang, Z. Exploring Atomic Defects in Molybdenum Disulphide Monolayers. *Nat. Commun.* **2015**, *6*, No. 6293.
(34) Qiu, H.; Xu, T.; Wang, Z. L.; Ren, W.; Nan, H. Y.; Ni, Z. H.; Chen, Q.; Yuan, S. J.; Miao, F.; Song, F. Q.; Long, G.; Shi, Y.; Sun, L. T.; Wang, J. L.; Wang, X. R. Hopping Transport Through Defect-Induced Localized States in Molybdenum Disulphide. *Nat. Commun.* **2013**, *4*, No. 2642.
(35) Salehi, S.; Saffarzadeh, A. Optoelectronic Properties of Defective MoS_2 and WS_2 Monolayers. *J. Phys. Chem. Solids* **2018**, *121*, 172−176.

https://doi.org/10.1021/acs.jpcc.1c01550
J. Phys. Chem. C 2021, 125, 8712−8718